Scientific paper

Synthesis, Characterization and Evaluation of Antimicrobial, Antioxidant & Anticancer Activities of Copper Doped Zinc Oxide Nanoparticles

Saranya Rishikesan[1] and Mubarak Ali Muhamath Basha[2,*]

[1] *Research and Development Centre, Department of Chemistry, Bharathiar University, Coimbatore - 641 046, Tamilnadu, India.*

[2] *Department of Chemistry, Chikkaiah Naicker College, Erode - 638 004, Tamil Nadu, India.*

** Corresponding author: E-mail: mubarakscience@gmail.com*
Contact Number: 091-9443312819

Received: 07-01-2019

Abstract

The present work reveals the influence of copper (Cu) doping in band gap energy level as well as selective cytotoxicity of ZnO nanoparticles against human breast cancer cells (MCF7), human cervical carcinoma (HeLa), and one normal (Vero) cell line. Cu-doped ZnO nanoparticles (Cu-ZnO NPs) were synthesized and validated by UV-Vis, FT-IR, XRD, SEM and EDAX. Cu-doping diminished the band gap energy of ZnO NPs from 3.54 eV to 3.29 eV. Antimicrobial activity has been evaluated against three bacterial and fungal strains. Antioxidant activity was examined using a DPPH free radical, $ABTS^+$ radicals, hydroxyl radicals and nitric oxide scavenging assay. Cu-ZnO NPs showed anticancer activity with IC_{50} value of 219.56 μg/mL against MCF7 and 137.27 μg/mL against HeLa cell lines. The doping of Cu with ZnO improved the selective cytotoxicity of ZnO NPs towards MCF7 and HeLa cells without affecting the normal cells.

Keywords: Cu-ZnO NPs, Antimicrobial activity, Cytotoxicity, MCF7, HeLa and Vero cell lines

1. Introduction

Cancer is a deadly disease which increases the mortality rate in the recent decades. Though the treatment of cancer by chemotherapy, radiation therapy and surgery were efficient towards the killing of cancer cells, it has an adverse effect towards the normal cells also.[1–3] The importance of these therapies is now gradually diminished due to the advancement of nanomedicine, targeted drug delivery and multi-target inhibitors.[4] Engineered nanoparticles (NPs) have advanced imaging, therapeutic activity and effective for early detection of cancer and cancer treatment.[5–8] It has the additional benefits of active/passive targeting, high solubility/bioavailability, biocompatibility and multi-functionality over traditional cancer therapies.[9] ZnO nanoparticles have multiple properties including favorable band gap, electrostatic charge, large surface area and potentiation of redox-cycling cascades.[10, 11] These characteristics of ZnO nanoparticles are being exploited in biomedical field such as cell imaging, bio-sensing and drug delivery. Recently, ZnO nanoparticles receive much attention for their potential application in cancer therapy. ZnO nanoparticles exhibited a preferential ability to kill human cancer cells as compared with normal cells.[12,13] ZnO nanoparticles have potential to develop as an anticancer candidate. The possible mechanism of cytotoxicity of ZnO NPs was associated with the occurrence of apoptosis.[14] However, for practical therapeutic applications, new strategies are required to further improve the cancer killing ability of ZnO nanoparticles without affecting normal cells. This study focuses on improving the cancer cells killing ability of ZnO nanoparticles by metal ions doping.

As the functionality and efficiency of ZnO nanostructures can be improved by increasing and modifying their surface area by adding some dopants materials i.e. biomolecules and transition metals (Mn, Fe, Cr, Cu) at nanoscale.[15,16] Through surface modification with biomolecules and transition metals, ZnO nanoparticles could be used as biosensors, antimicrobial, antioxidants, drug delivery systems and bio-imaging materials.[16–18] Different methods have been developed for the fabrication of ZnO and transition metal doped ZnO nanoparticles.[19] Among all the dopants, doping of ZnO NPs with Cu greatly alter

the optical, morphological structural, magnetic, electrical, and biological properties of the ZnO NPs.[20,21] ZnO NPs doped with Cu have shown remarkable improvement in different properties i.e. electrical conductivity,[22] magnetic,[23] biological,[24] gas sensing,[25] optical properties and mechanical strength.[26] Cu-doped ZnO NPs showed enhanced anticancer activity as compared to Un-doped ZnO NPs.[27]

The present study aims on improving the anticancer activity of ZnO NPs by cationic doping. Especially, Cu was considered as one of the most effective doping elements for improving the anticancer activity of ZnO NPs. It was found that the doped Cu^{2+} ions with half-filled electronic configuration which contributed to the enhanced anticancer activity of ZnO nanoparticles. In order to verify the efficacy of copper doping with ZnO in various aspects an attempt was taken to investigate elaborately. Herein, we report the synthesis, characterization of ZnO and Cu-ZnO nanoparticles and its antimicrobial, antioxidant and anticancer activities.

2. Experimental

2. 1. Materials

All chemicals used were of analytical grade and used as received. Zinc sulphate heptahydrate ($ZnSO_4 \cdot 7H_2O$), Sodium hydroxide (NaOH), Copper sulphate pentahydrate ($CuSO_4 \cdot 5H_2O$) were purchased from Merck and were used as received.

2. 2. Synthesis of ZnO NPs

$ZnSO_4 \cdot 7H_2O$ (0.4 M) and NaOH (0.8 M) were dissolved in distilled water. ZnO nanoparticles was prepared using co-precipitation method by dropwise addition of NaOH to $ZnSO_4 \cdot 7H_2O$ with constant stirring at 80 °C until a white precipitate was formed. After cooling, the precipitate was washed several times with deionized water followed by ethanol and dried in a hot air over for 5 h at 80 °C. The dried samples were calcined at 350 °C for 3h to obtain the nano sized ZnO.

2. 3. Synthesis of Cu-ZnO NPs

$ZnSO_4 \cdot 7H_2O$ (0.8 M) was dissolved in deionized water. Cu-ZnO NPs were prepared by the drop wise addition of NaOH (0.8 M) solution and $CuSO_4 \cdot 5H_2O$ (0.02 M) solution to $ZnSO_4 \cdot 7H_2O$ with constant stirring. The stirring was continued until the complete precipitation occurs. Before filtration the mother liquid was aged for 12 h. The residue thus obtained was dried at 80 °C for 12 h and calcined at 350 °C for 3 h.

2. 4. Characterization Methods

The Ultra Violet-Visible-Diffuse reflectance spectroscopy (UV-Vis-DRS) measurements were performed with a JASCO V-550 double beam spectrophotometer with PMT detector. The samples were filled in a quart's cuvette of 1 cm light-path length, and the light absorption spectra were given in reference to deionized water. Surface structure was characterized by a Fourier Transform Infrared (FT-IR) spectrophotometer (JASCO-RT-IR-460 plus). The present study is restricted to the assignment of various vibrational modes of metal oxides compounds within the frequency range 400–4000 cm^{-1} and IR analysis was carried out for oven-dried samples. The sample for IR analysis was prepared by mixing 0.1 g of KBr with 0.003 g of sample and then pressing into a pellet. X-ray diffraction (XRD) patterns were collected at 25 °C using (XPERT-PRO-X-RAY diffractometer with Cu-Kα radiation and structural assignments were made with reference to the JCPDS powder diffraction files. Scanning electron microscopy (SEM) images were performed by JSM-6701F-6701 instrument in both back scattered electron modes. The elemental analysis was detected by an energy dispersive X-ray spectroscopy (EDX) attached to the SEM.

2. 5. Antimicrobial Activity

Antibacterial and antifungal activities were evaluated for the synthesized ZnO and Cu-ZnO NPs. The salt of $ZnSO_4 \cdot 7H_2O$, $CuSO_4 \cdot 5H_2O$ and the synthesized NPs of ZnO and Cu-ZnO were tested to determine their antimicrobial activities against three bacterial strains namely *E. coli* (1B), *S. aureus* (2B) and *P. aeruginosa* (3B) and three fungal strains namely *Aspergillus flavus (1F)*, *Candida albicans (2F)* and *Fusarium (3F)*. The samples were dissolved in dimethyl sulphoxide and it was made into the required concentrations. The bacterial strains as well as fungal strain were inoculated separately in 30 mL of nutrient broth in a conical flask and incubated for 24 h to get active strain by using well diffusion method. Muller Hinton agar was poured separately into petri dishes. After solidification 0.25 mL of test strains were inoculated in the media separately and care was taken to ensure proper homogenization. The experiment was performed under strict aseptic conditions. After the medium solidified, a well was made in the plates with sterile borer (5mm). The (40 μL) of the test sample was introduced into the well and plates were incubated at 37 °C for 72 h. All samples were tested in triplicates. Microbial growth was determined by measuring the diameter of zone of inhibition. Amikacin and Ketoconazole were used as control for antibacterial and antifungal activity assay respectively.

2. 5. 1. Determination of Minimum Inhibitory Concentration (MIC)

A sterile 96 well plates were prepared under aseptic conditions. The freshly prepared sample suspensions in DMSO were sonicated using a sonicator. A volume of 100 μL of test material in 10% DMSO (a stock concentration of

1 mg/mL for purified compounds) was pipetted into the first row of the plate. To all the other wells, 50 µL of nutrient broth was added for bacteria cells and 50 µL of Sabouraud dextrose broth for fungi cells, and serial dilutions were performed using a multichannel pipette. To each well, 10 µL of resazurin indicator solution was added. Finally, 10 µL of bacterial/fungal suspension (5×10^6 cfu/mL) was added to each well to achieve a concentration of 5×10^5 cfu/mL. The commercial drugs Amikacin (against bacteria) and Ketoconazole (against fungi) were used as a positive control. The plates were prepared in triplicate, and placed in an incubator set at 37 °C for 18–24 h and the color change from purple to pink or colorless indicates the reduction of dye by the viable bacteria/fungi. The lowest concentration at which color change occurred was taken as the MIC value. The average of three values was calculated to get MIC values.

2. 6. Evaluation of Antioxidant Properties of the Compounds

The remarkable antibacterial and antifungal activities of the synthesized Cu-ZnO NPs induced us to study its radical scavenging properties. The radical scavenging activities of Cu-ZnO NPs along with standard have been examined with reference to 2-20-diphenyl-1-picrylhydrazyl (DPPH) radicals, 2, 2′-azino-bis (3-ethyl benzothiazoline-6-sulfonic acid (ABTS) radicals, hydroxyl radicals (·OH) and nitric oxide (NO·) assay and the determination of 50% activity (IC_{50}) values.

2. 6. 1. DPPH free Radical Scavenging Assay

The DPPH radical scavenging activity of Cu-ZnO NPs was measured according to the method of Blios.[28] The DPPH radical is a stable free radical having λ_{max} at 517 nm. A variable concentration of the sample (20–100 µg/mL) were mixed with 1.0 mL of methanolic solution containing DPPH radicals, resulting in the final concentration of DPPH being 0.2 mM. The mixture was shaken vigorously and left to stand for 30 min, and the absorbance was measured at 517 nm. Vitamin E was used as control. The percentage of inhibition in DPPH radical scavenging activity was calculated as follows;

$$\% \text{ Inhibition} = (A_0 - A_1)/A_0 \times 100$$

2. 6. 2. ABTS Cation Radical Scavenging Assay

ABTS decolorization assay involves the generation of the $ABTS^+$ chromophore by the oxidation of ABTS with potassium persulphate. It is applicable for both hydrophilic and lipophilic compounds. The scavenging activity of Cu-ZnO NPs on ABTS cation radical was measured at 734 nm.

Equal volume of 7 mM of ABTS was mixed with 2.45 mM potassium persulphate and the mixture was allowed to stand in the dark at room temperature for 12–16 h before use. $ABTS^+$ solution was diluted to an absorbance of 0.7 ± 0.05 with ethanol at 734 nm. The reaction was initiated by the addition of 1.0 mL of diluted $ABTS^+$ to 10 µL of different concentrations (20–100 µg/mL) of sample. Vitamin E was used as standard and positive control. The absorbance was read at 734 nm and the percentage inhibitions were calculated. The inhibition was calculated according to the equation,

$$I = (A_0 - A_1)/A_0 \times 100$$

Where, A_0 is absorbance of control reaction, A_1 is absorbance of test compound.

2. 6. 3. Hydroxyl Radical Scavenging Assay

The hydroxyl radical scavenging activities of the compounds have been investigated using Nash method.[29] A reaction mixture of 3.0 mL volume contained, 1.0 mL of 1.5 mM $FeSO_4$, 0.7 mL of 6 mM hydrogen peroxide, 0.3 mL of 20 mM sodium salicylate and 1.0 mL of different concentrations (50–250 µg/mL) of Cu-ZnO NPs. After incubation for an hour at 37 °C, the absorbance of the hydroxylated salicylate complex was measured at 562 nm. Vitamin E was used as positive control. The percentage scavenging effect was calculated as,

$$\text{Scavenging activity} = [1 - (A_1 - A_2)/A_0] \times 100$$

Where, A_0 is absorbance of the control, A_1 is absorbance in the presence of the extract; A_2 is absorbance without sodium salicylate.

2. 6. 4. Nitric Oxide (NO) Assay

The amount of nitrite was determined by the literature method.[30] The reaction mixture (6.0 mL) containing sodium nitroprusside (4.0 mL), phosphate buffer saline (PBS, 1.0 mL) and different concentrations (50–250 µg/mL) of a sample (1.0 mL) in DMSO was incubated at 25 °C for 15 minutes. After incubation, 1.0 mL of sulphanilic acid reagent was added, mixed well and allowed to stand for 5 minutes for completion of diazotization and 1.0 mL of N-(1-naphthyl) ethylenediamine dihydrochloride was added, mixed well and allowed to stand for 30 minutes in diffused light. A pink colored chromophore was formed. The absorbance of these solutions was measured at 540 nm against corresponding blank solutions. Vitamin E was used as a standard.

The inhibition was calculated according to the equation, $I = (A_0 - A_1)/A_0 \times 100$

2. 7. Anticancer Activity of Cu-ZnO NPs

The MCF7 and HeLa cells were grown in Eagle's minimum essential medium containing 10% fetal bovine serum (FBS) while Vero cells were grown in Dulbecco's modified Eagle's medium (DMEM) containing 10% FBS. 100 µL per well of cell suspension were seeded into 96-well

plates at plating density of 10,000 cells/well and incubated to allow for cell attachment at 37 °C, 5% CO_2, 95% air and 100% relative humidity. After 24 h the cells were treated with serial concentrations of the test samples (Cu-ZnO NPs). Cu-ZnO NPs were initially suspended in neat dimethylsulfoxide (DMSO) and an aliquot of the sample solution was diluted to twice the desired final maximum test concentration with serum free medium. Additional four serial dilutions were made to provide a total of five sample concentrations. Triplication was maintained, and the medium without the test sample served as the control. After 24 h, the wells were treated with 20 μL MTT [5 mg mL^{-1} phosphate buffered saline (PBS)] and incubated at 37 °C for 4 h. The medium with MTT was then removed separately and the formed formazan crystals were dissolved in 100 mL DMSO. The absorbance at 570 nm was measured using an ELISA plate reader. The graph was plotted between the percentage of cell inhibition and the concentration of the complexes. IC_{50} values were calculated from the percentage of inhibition. The percentage of cell inhibition was determined using the formula which is given below,

% inhibition = [mean OD of untreated cells (control)/mean OD of treated cells (control)] × 100

3. Results and Discussion

3. 1. Ultra Violet-Visible-Diffuse Reflectance Spectroscopy (UV-Vis –DRS)

Fig. 1 depicts the UV-Vis DRS of ZnO and Cu-ZnO NPs. There are four bands at 213, 255, 358 and 448 nm for ZnO nanoparticles. In Cu-ZnO NPs the bands around 200–360 nm remained unaltered.

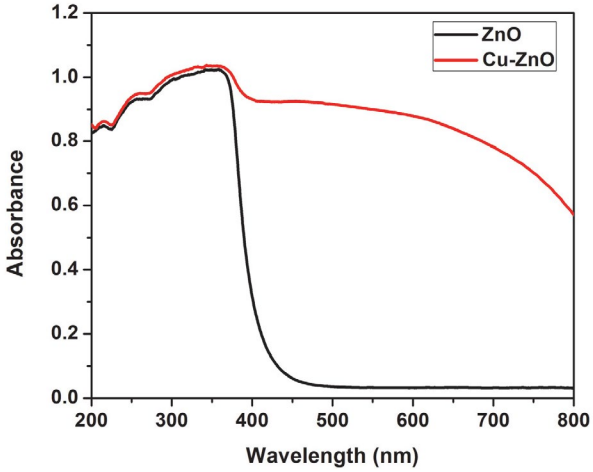

Figure 1. UV-Vis DRS spectra of ZnO and Cu-ZnO NPs

The band which is appeared at 448 nm is shifted to 464 nm. A slight red shift observed in the case of Cu-ZnO is due to the doping of Cu into the crystal lattice of Zn. The red-shift in absorption peak showed decrease in band gap of ZnO with Cu doping. The band gap of ZnO NPs was decreased from 3.54 to 3.29 eV after doping with copper. Fig. 2 shows the Tauc's plot of ZnO(a) and Cu-ZnO(b). The observed redshift in band gap (Eg) is due to Cu doping-induced band-edge bending. The change in the band gap energy is attributed to two reasons: First, the sp–d exchange interactions between sp and d orbitals of host and dopant, respectively, lead to negative correction in the conduction band and positive correction in valence band, hence overall band narrowing is observed.[31,32] Secondly, the electronegativity of Cu is 1.9 as compared to ZnO which is 1.6, leading to a chemical affect in the host ZnO crystal which results in decrease in band gap.

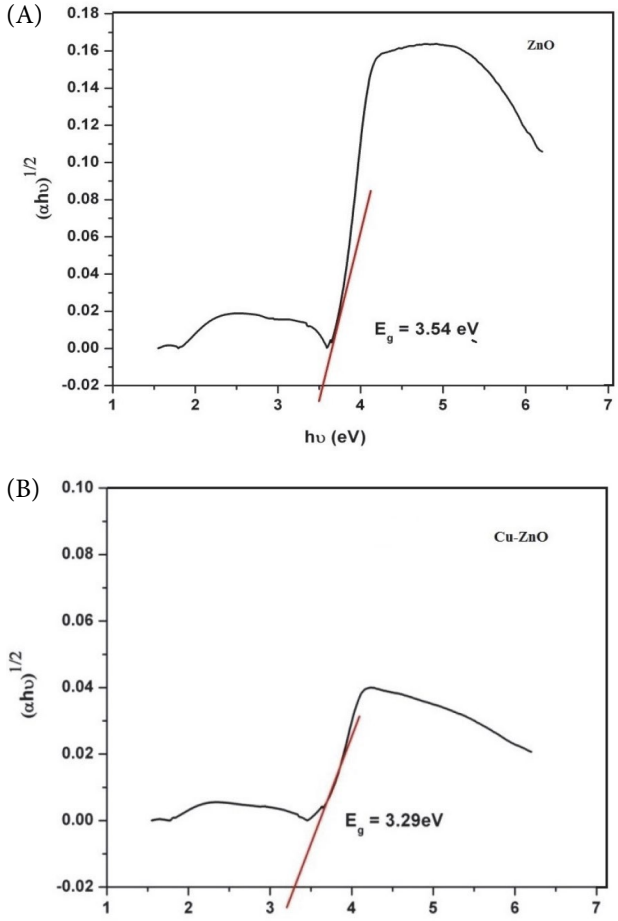

Figure 2. (A) and (B) τ-Plot of ZnO, and Cu-ZnO NPs respectively

3. 2. FT-IR Spectral Studies

The FT-IR spectra of ZnO and Cu-ZnO NPs are represented in Fig 3. The peak observed at 3448 and 1132 cm^{-1} are attributed to O–H stretching vibration of H_2O in the Cu–Zn–O lattice. The peak at 570 cm^{-1} is attributed to Zn–O[33,34] whereas in the copper doped ZnO the corresponding peak is observed at 561 cm^{-1}.[35]

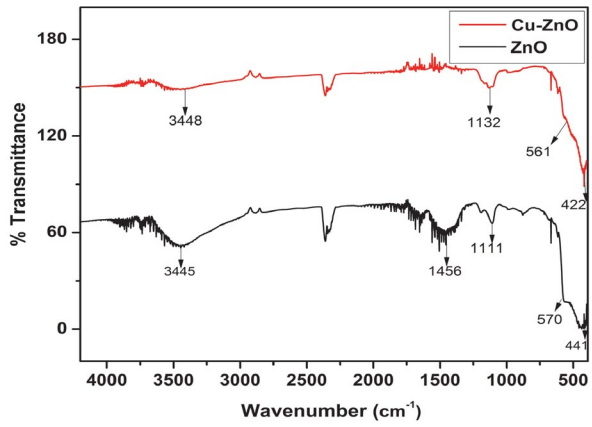

Figure 3. FT-IR data of ZnO and Cu-ZnO NPs

3. 3. X-RAY Diffraction (XRD) Analysis

The XRD pattern of ZnO, Cu-ZnO is depicted in Fig. (4 & 5) All the diffraction peaks can be assigned to the ZnO crystal phase with a hexagonal wurtzite structure (JCPDS-36-1451). The sharp and intensive diffraction peaks indicated that products were well crystallized. The average crystallite size was calculated from Debye-Scherrer formula.[36] The average crystallite size of ZnO and Cu-ZnO are 30 nm and 27 nm respectively. From the XRD investigation, the crystal structure of ZnO and Cu-ZnO is wurtzite. The lattice constant for ZnO and Cu-ZnO are a = 0.3247 nm, c = 0.5203 nm and a = 0.3249 nm, c = 0.5204 nm respectively. The very slight shift in peak positions were observed with copper doping in ZnO indicating that all doped copper occupied the substitution sites. No secondary phases viz., Cu_2O, CuO, or other metallic Cu or Zn phases were observed. It is noteworthy that no copper oxide related peak could be observed in the XRD spectra. One probable reason was that the concentration of doped Cu was so low that it cannot be detected by XRD. The other reason was that the radius of Cu-ion (0.073 nm) is similar to that of Zn-ions (0.074 nm) and the Cu-ions may be incorporated into the lattice of ZnO structure.[37] Fig. 5 also shows that Cu-ions doping has almost no influence on the phase structure of ZnO. The intensity of XRD peaks of Cu-ZnO NPs was decreased in comparison to that of pure ZnO which indicates a decrease in crystallinity of ZnO with Cu doping. The decrease in crystallite size implies that doping with Cu restrains increase of grain size and refines the crystal size.

3. 4. Scanning Electron Microscope (SEM) Analysis

The morphology of ZnO, Cu-ZnO NPs was elucidated by SEM analysis. SEM micrographs of ZnO, and Cu-ZnO are depicted in Fig.6 (A-D). It was clearly observed that the particles were spherical in shape and well dispersed.

ZnO structure was observed like a stack of vertically aligned thin nanosheets whereas Cu-ZnO possessed rods and grain like structures. The average grain size of all the samples is in the range of 40–60 nm. Cu doping strongly influences the grain size and morphology of ZnO nano-

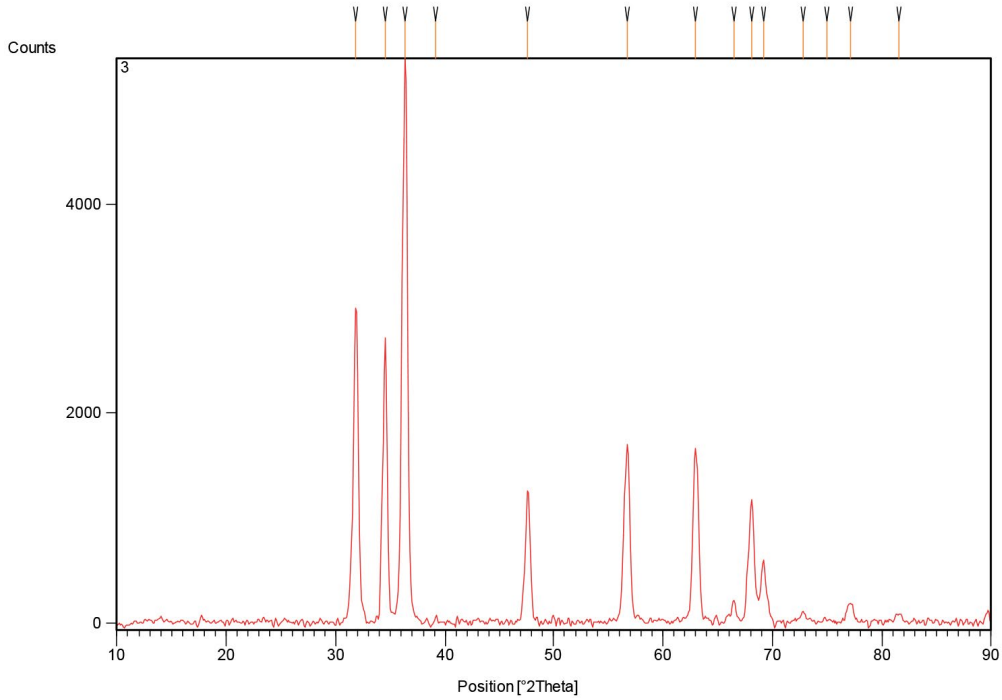

Figure 4. XRD pattern of ZnO NPs

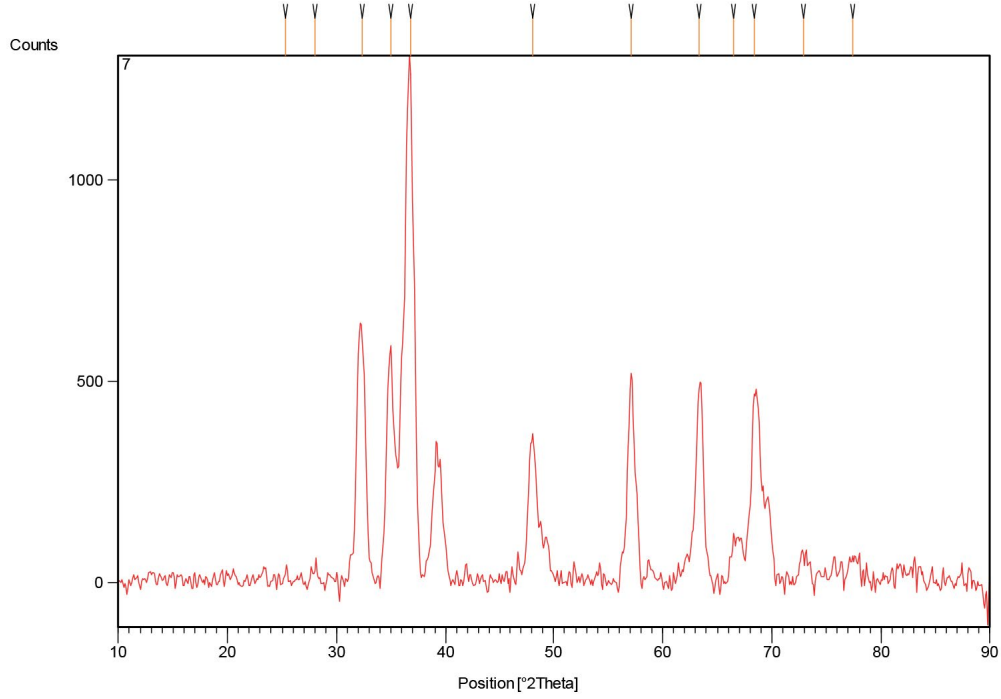

Figure 5. XRD pattern of Cu-ZnO NPs

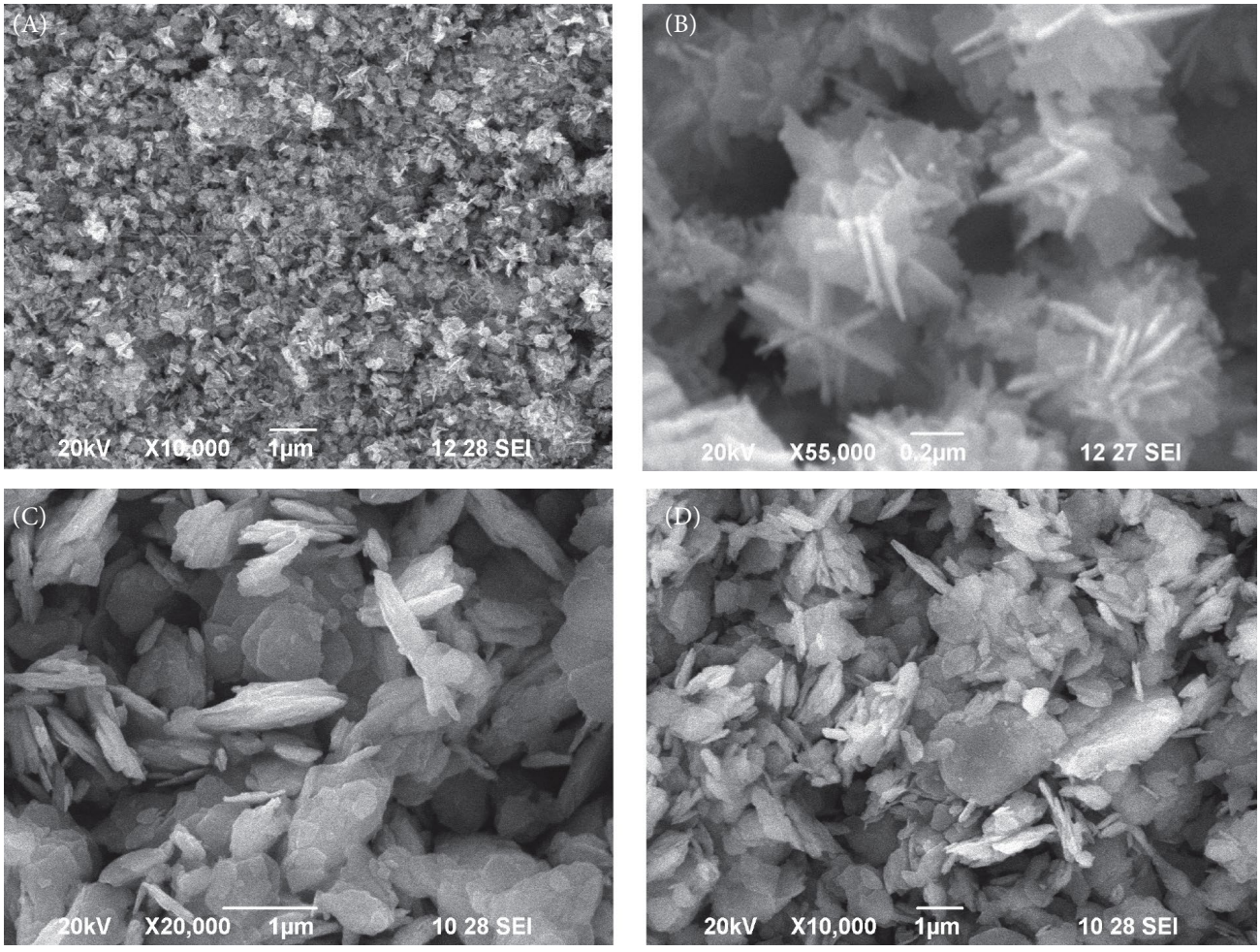

Figure 6. SEM images of ZnO (A) and Cu-ZnO (B-D)NPs at various magnification

particles. The average particle size was found to decrease with the increase in Cu doping into the ZnO matrix. The decrease in the particle size was mostly ascribed to the formation of Cu–O–Zn on the surface of the doped nanoparticles, which prevents the growth of crystal grains and assists separation of particles.[38]

3. 5. Energy-Dispersive X-ray Analysis (EDAX)

EDAX was carried out to analyze the chemical composition and formation of un-doped ZnO and Cu-ZnO NPs. EDAX was used to confirm the presence of cationic metal ion (Cu^{2+}) dopant in ZnO. Fig. 7 shows the EDAX spectrum of ZnO (a) and Cu-ZnO (b). In addition, the EDAX spectra confirmed the presence of chemical constituents (Zn = 72.96% and O = 27.04% in un-doped ZnO NPs; Cu = 3.21%, Zn = 52.71% and O = 39.12% in Cu-ZnO NPs, it was also found that sample Cu-ZnO was composed only by Zn, Cu and O without any other impurities. The EDAX peak positions were consistent with ZnO, and the sharp peaks of EDAX indicated that the synthesized NPs had crystalline structures.[39,40] The strong intensity and narrow width of ZnO diffraction peaks indicate that the resultant products were highly crystalline in nature. These findings were in close agreement with previous reports[41] but with slight difference due to variations in chemical composition.

3. 6. Antimicrobial Activity

Comparative analysis of the antimicrobial efficacy of ZnO and Cu- ZnO NPs was carried out using well diffusion method and the results are tabulated in Tables 1 and 2. The antibacterial activity of ZnO and Cu-ZnO NPs was studied against three bacterial strains such as 1B, 2B, 3B and three fungal strains 1F, 2F and 3F. The zone of inhibition (mm) was evaluated for three concentrations such as 50 µL, 75 µL and 100 µL. It was clearly indicated that the percentage enhancement of the activity for 1B was 60% in the case of 50 µL. But in the case of 2B and 3B were 70.5% and 75% respectively. The results showed that the Cu-ZnO showed good inhibitory action against 3B. In the second case (75 µL) the percentage of enhancement of 1B, 2B and 3B were 62.5%, 72.2% and 80.9% respectively.

Table 1. Antibacterial activity of Cu-ZnO NPs

Name of the Sample	**Zone of inhibition in mm**								
	E.coli			***Pseudomonas aerugenousa***			***Staphylococcus aeureus***		
	50 µL	**75 µL**	**100 µL**	**50 µL**	**75 µL**	**100 µL**	**50 µL**	**75 µL**	**100 µL**
ZnO	12 ± 0.5	13 ± 0.8	14 ± 0.2	11 ± 0.4	12 ± 0.9	13 ± 0.7	10 ± 0.8	12 ± 0.1	13 ± 0.6
Cu-ZnO	16 ± 0.9	17 ± 0.4	18 ± 0.1	16 ± 0.4	17 ± 0.1	17 ± 0.9	15 ± 0.3	16 ± 0.5	17 ± 0.2
Amikacin	18 ± 0.2	20 ± 0.45	22 ± 0.3	17 ± 0.8	19 ± 0.2	21 ± 0.5	16 ± 0.9	18 ± 0.8	20 ± 1.2

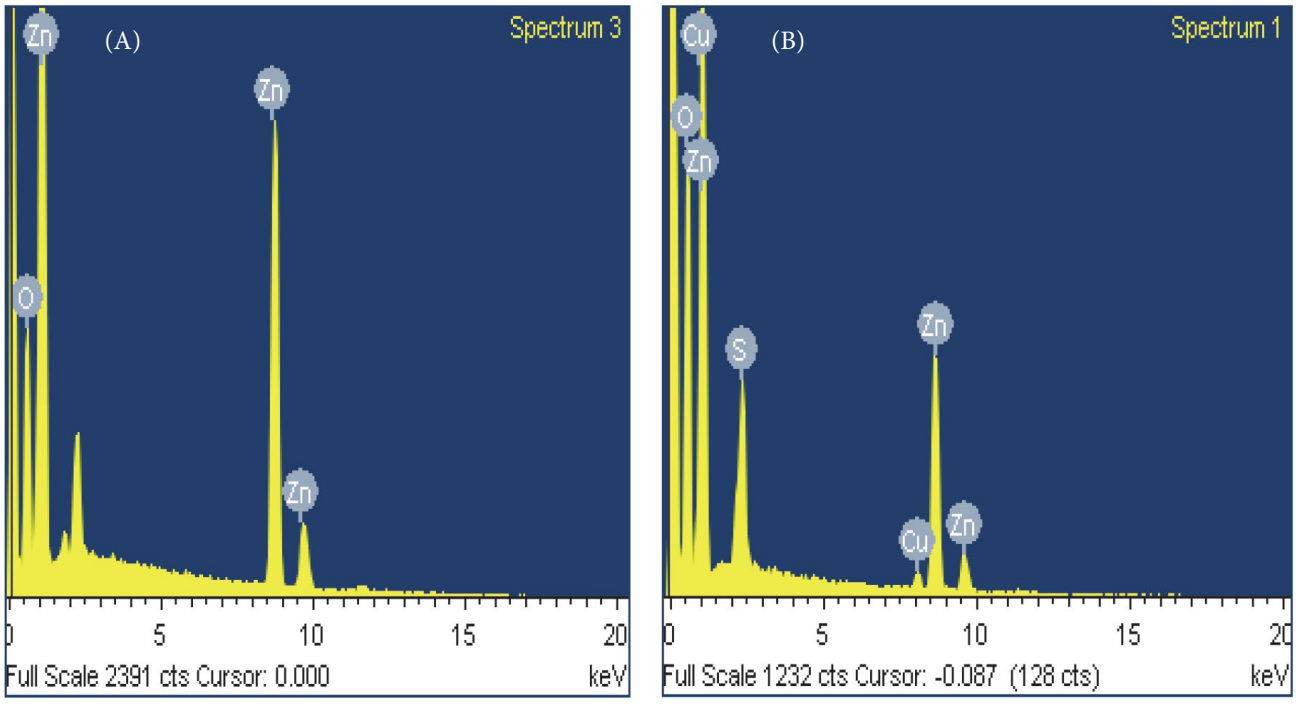

Figure 7. EDAX spectra of (A) ZnO and (B) Cu-ZnO NPs

Table 2. Antifungal activity of Cu-ZnO NPs

Name of the Sample	Zone of inhibition in mm								
	Aspergillus flavus			*Candida albicans*			*Fusarium sp*		
	50 µL	**75 µL**	**100 µL**	**50 µL**	**75 µL**	**100 µL**	**50 µL**	**75 µL**	**100 µL**
ZnO	13 ± 0.1	15 ± 0.4	17 ± 0.56	12 ± 0.3	14 ± 0.2	15 ± 1.0	12 ± 0.8	14 ± 1.0	17 ± 0.1
Cu-ZnO	17 ± 0.4	18 ± 0.7	20 ± 1.0	16 ± 0.8	17 ± 0.9	19 ± 1.0	17 ± 0.1	18 ± 0.3	19 ± 0.9
Ketoconazole	20 ± 0.6	22 ± 0.3	24 ± 0.4	19 ± 0.6	21 ± 0.3	23 ± 0.1	20 ± 0.2	22 ± 0.05	24 ± 0.3

It was revealed that the zone of inhibition (%) was increased with concentration. If concentration increased to 100 µL, the percentage of enhancement of 1B, 2B and 3B were 64.7%, 73.6% and 86.3% respectively.

Similarly, the antifungal activity of ZnO and Cu-ZnO has been investigated systematically. Additionally, the zone of inhibition (mm) has been evaluated for three kinds of fungal species such as 1F, 2F and 3F. In this connection, three concentrations such as 50 µL, 75 µL and 100 µL were taken for the analysis. The percentage of enhancement was also calculated. From the results, the percentage of enhancement for 1F, 2F and 3F were 76.4%; 7% and 73.3% respectively. On increasing the concentration to 75 µL and 100 µL, the zone of inhibition increases. However, the percentage of enhancement from ZnO to Cu-ZnO was 83.3% (1F), 82.3% (2F) and 75% (3F) respectively. The results indicated that the percentage of enhancement was observed maximum for Cu-ZnO (100 µL concentration) against 1F.

The results revealed that both ZnO and Cu-ZnO NPs were effective antibacterial agents on gram-positive as well as on gram-negative bacteria. However, percentage reduction in bacterial growth was found to be significantly higher using Cu-ZnO NPs compared to that of the ZnO NPs. Thus, the antibacterial effect of ZnO and Cu-ZnO was more pronounced for gram-positive bacteria as compared to gram-negative bacteria, which was in good agreement with the earlier studies.[31,42–44] This was explained on the basis of differences in (i) cell membrane structure, (ii) physiology and metabolic activities of the cell, and (iii) degree of contact of gram-positive and gram-negative bacteria.[45] The antibacterial activity of pure and iron-doped ZnO nanoparticles showed that they were more resistant to gram-negative bacteria than gram-positive bacteria. The results were in good agreement with our results.[46]

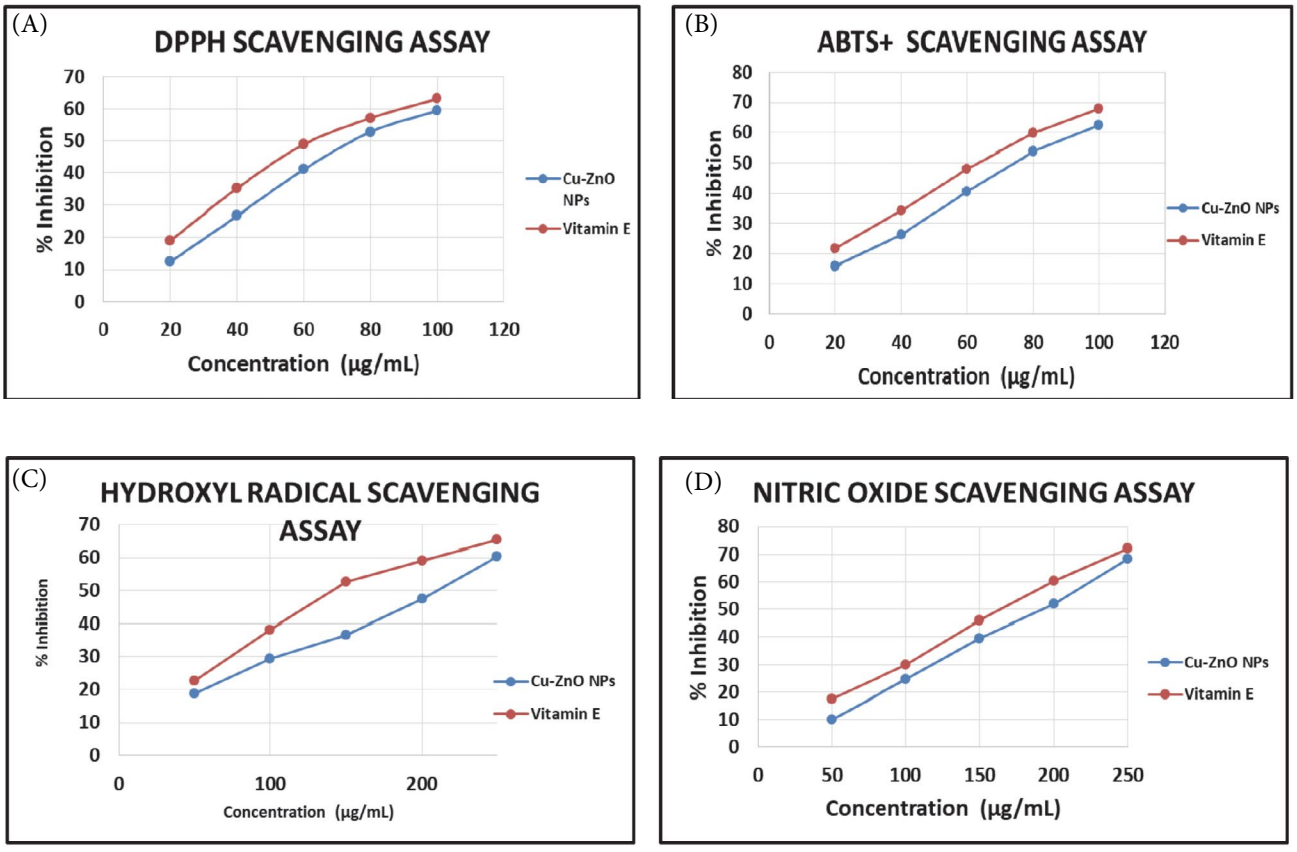

Figure 8. (A) DPPH, (B) $ABTS^{+}$, (C) · OH, (D) NO· radical scavenging activities of Cu-ZnO NPs and standard at various concentrations.

3. 7. Antioxidant Activity

The antioxidant activity of Cu-ZnO NPs were evaluated in a series of *in vitro* assays involving DPPH radicals, ABTS cationic radicals, hydroxyl radicals, nitric oxide scavenging assay in a dose dependent manner. The antioxidant activities of the Cu-ZnO NPs along with the standard at various concentrations have been shown in Fig.8 respectively. The IC_{50} values of Cu-ZnO NPs in relevance to DPPH, $ABTS^+$, ·OH, NO· assays were 76.29, 74.07, 205.96 and 180.89 µg/mL respectively (Table 3). From the results, the minimum and maximum percentage of inhibition for Cu-ZnO NPs against DPPH radicals for the concentration of 20 µg/mL and 100 µg/mL were 12.54 ± 0.28 and 59.45 ± 0.16 respectively. $ABTS^+$ scavenging assay was also carried out to evaluate the free radical scavenging activity of the synthesized Cu-ZnO NPs. The minimum and maximum percentages of inhibition for 20 µg/mL and100 µg/mL concentrations were 15.75 ± 0.26 and 62.48 ± 0.18 respectively. In the case of hydroxyl radicals scavenging assay, the free radical scavenging activity was investigated using various concentrations such as 50 µg/mL, 100 µg/mL, 150 µg/mL, 200 µg/mL and 250 µg/mL. The scavenging activity was increased with concentration as expected. The minimum and maximum percentage of inhibition at the concentrations of 50 µg/mL and 250 µg/mL were 18.61 ± 0.23 and 60.45 ± 0.55 respectively. Nitric oxide scavenging assay was also carried out for evaluation of free radical scavenging activity of Cu-ZnO NPs. The minimum and maximum percentage of inhibition at the concentration 50µg/mL and 250µg/mL were 10.15 ± 0.61 and 68.36 ± 0.94 respectively. The results indicated that the synthesized Cu-ZnO NPs exhibited appreciable antioxidant activity. The results were compared with the standard Vitamin E. The comparison clearly indicated that the Cu-ZnO NPs exhibited comparable activity with that of the standard. The results revealed that a concentration dependent activity was observed.

Table 3. IC_{50} values (in µg/mL) calculated from various radical scavenging assays of Cu-ZnO NPs and standard vitamin E

Compound	DPPH	ABTS	·OH	NO·
Cu-ZnO	76.29	74.07	205.96	180.89
Vitamin E	63.32	63.14	147.88	158.13

3. 8. Anticancer Activity

The *in vitro* cytotoxic activity of the compound was determined against human breast (MCF7), human cervical (HeLa) cancer and Vero cell lines using MTT assay. Figure 9 showed the cytotoxicity of the ZnO NPs after 48 h incubation on MCF7, HeLa and Vero cell lines respectively. The results were analyzed by means of cell inhibition expressed as IC_{50} values. Cu-ZnO NPs showed only moderate activity with IC_{50} value of 219.56 and 137.27 µg/mL against MCF7 and HeLa cell lines respectively. Fortunately, Cu-ZnO NPs are less toxic towards the normal cell line which was evident from its high IC_{50} value (> 300 µg/mL). This showed that our Cu-ZnO NPs are particularly toxic towards cancer cell lines.

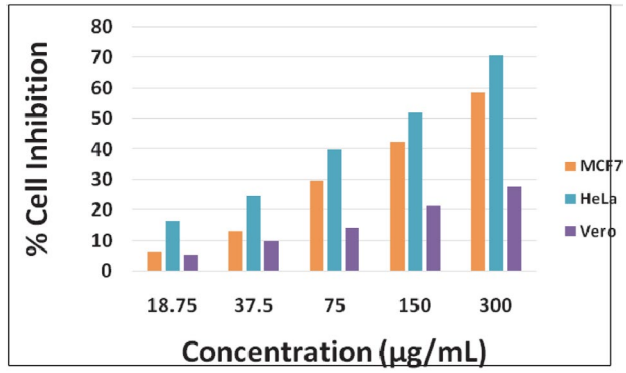

Figure 9. Cytotoxicity of Cu-ZnO NPs in MCF7, HeLa and Vero cell lines

4. Conclusions

In the present work, we have accomplished the synthesis of ZnO and Cu-ZnO nanoparticles. The antibacterial and antioxidant activity of the synthesized ZnO and Cu-ZnO NPs were investigated. The anticancer activity of Cu-ZnO NPs was also evaluated. Cu-ZnO NPs showed superior antibacterial action against grampositive as well as gram-negative bacteria. In addition, doped ZnO NPs had shown appreciable antioxidant activity against DPPH, $ABTS^+$, ·OH and NO· assays. The UV–Visible results revealed that band gap undergoes a red-shift in doped ZnO nanorods as compared to pure ZnO. We infer that strong bonding of Cu in the host lattice of ZnO was responsible for the significant reduction of ZnO nanoparticle dissolution. Cu-ZnO NPs exhibited moderate anticancer activity against the tested cell lines. One of the important findings of this study was that Cu-doping unaltered the benign nature of ZnO nanoparticles towards the normal (Vero) cells. Overall, our data suggested a novel approach through which the inherent selective cytotoxicity of ZnO NPs against human breast cancer cells (MCF7) and human cervical carcinoma (HeLa) can be improved by doping of Cu^{2+} ion. Further research on anticancer activity of Cu-ZnO NPs in different types of cancer cells is warranted.

5. Acknowledgements

Author thanks Dr. R. Karvembu, Department of Chemistry, National Institute of Technology, Tiruchirappalli for providing the lab facility.

6. References

1. G. Bisht, S. Rayamajhi, *Nanobiomedicine*. **2016**, *3,* 1–11. **DOI:**10.5772/63437
2. K. S. Smalley, M. Herlyn, *Mini Rev Med Chem*. **2006**, *6*, 387–393. **DOI:**10.2174/138955706776361402
3. R. Langer, *Nature.* **1998**, *392*, 5–10. **DOI:**10.1038/32020
4. R. Gowda, N. R. Jones, *J. Nanomed Nanotechnol.* **2013**, *4*, 184–219.
5. I. Baskaran, T. S. N. Sankara Narayanan, A. Stephen, *Mater. Lett.* **2006,** *60,*1990–1995. **DOI:**10.1016/j.matlet.2005.12.065
6. M. F. Serag, N. Kaji, S. Habuchi, A. Biancod, Y. Baba, *RSC Adv.* **2013**, *3*, 4856–4862. **DOI:**10.1039/c2ra22766e
7. S. Poyraz, I. Cerkez, T. S. Huang, Z. Liu, L. Kang, J. Luo, X. Zhang, *ACS Appl. Mater. Interfaces.* **2014**, *6*, 20025–20034. **DOI:**10.1021/am505571m
8. R. Wang, P. S. Billone, W. M. Mullett, *J. Nanomater*. **2013**, *2013*, 1–12. **DOI:**10.1155/2013/629681
9. S. E. McNeil, *Nanomed. Nanobiotechnol*. **2009**, *1*, 264–271. **DOI:**10.1002/wnan.6
10. M. J. Akhtar, H. A. Alhadlaq, A. Alshamsan, M. A. Majeed Khan, M. Ahamed, *Scientific Reports*. **2015**, *5,* 13876. **DOI:**10.1038/srep13876
11. J. W. Rasmussen, E. Martinez, P. Louka, D. G. Wingett, *Expert Opin. Drug Deliv*. **2010**, *9*, 1063–1077. **DOI:**10.1517/17425247.2010.502560
12. M. Premanathan, K. Karthikeyan, K. Jeyasubramanian, G. Manivannan, *Nanomed Nanobiotechnol.* **2011**, *7*, 184–192. **DOI:**10.1016/j.nano.2010.10.001
13. C. Hanley, J. Layne, A. Punnoose, K. M. Reddy, I. Coombs, A. Coombs, K. Feris, D. Wingett, *Nanotechnology*. **2008**, *19,* 295103–295113. **DOI:**10.1088/0957-4484/19/29/295103
14. A. B. Moghaddam, M. Moniri, S. Azizi, R. A. Rahim, A. B. Ariff, M. Navaderi and R. Mohamad, *Genes*. **2017**, *8*, 281–295. **DOI:**10.3390/genes8100281
15. S. A. Khan, F. Noreen, S. Kanwal, G. Hussain, *Dig J Nanomater Biostruct*. **2017**, *12*, 877–890.
16. K. Kalantar, K. Kabir, F. Gharibi, S. Hatami, A. Maleki, *J Med Bacteriol*. **2013,** *2*, 20–26.
17. R. Chauhan, A. Kumar, R. P. Chaudhary, *J Chem Pharm Res*. **2010,** *2*, 178–183.
18. G. Glaspell, P. Dutta, A. Manivanna, *J. Clust. Sci.* **2005,** *16*, 523–536. **DOI:**10.1007/s10876-005-0024-y
19. A. N. Malika, A. R. Reddy, K. S. Babu, K.V. Reddy, *Ceram. Int*. **2014**, *40*, 12171–12177.
20. S. Deka, P. A. Joy, *Solid State Commun*. **2007**, *142*, 190–194. **DOI:**10.1016/j.ssc.2007.02.017
21. R. Saleh, N. F. Djaja, *Spectrochim Acta A Mol Biomol Spectrosc*. **2014**, *130*, 581–590. **DOI:**10.1016/j.saa.2014.03.089
22. O. G. Jayakumar, H. G. Salunke, R. M. Kadam, M. Mohapartra, G. Yaswant, S. K. Kulshreshtha, *Nanotechnology*. **2006**, *17*, 1278–1285. **DOI:**10.1088/0957-4484/17/5/020
23. M. E. Abrishami, A. Kompany, S. M. Hosseini, N. G. Bardar, *J Solgel Sci Technol.* **2012**, *62*, 153–159. **DOI:**10.1007/s10971-012-2701-2
24. S. Kim, J. H. Jun, K. Chao, J. Yun, K. S. Suh, T. Y. Kim, *Organic Electron*. **2008**, *9,* 445–451. **DOI:**10.1016/j.orgel.2008.02.001
25. Y. Lu, J. Zhong, S. Muthukumar, Y. Chen, H. M. Ng, W. Jiang, E. L. Garfunkel, *Appl Phys. Lett*. **2003**, *83*, 3401–3403. **DOI:**10.1063/1.1621729
26. D. Meng, X. Yu, C. Liu, X. He, Y. Wang, J. Xie, *Material Letter*. **2012**, *86*, 112–114. **DOI:**10.1016/j.matlet.2012.07.040
27. S. A. Khan, F. Noreen, S. Kanwal, A. Iqbal, G. Hussain, *Mater. Sci. Eng. C.* **2018**, *82,* 46–59. **DOI:**10.1016/j.msec.2017.08.071
28. M. S. Blois, *Nature.* **1958**, *29*, 1199–1200. **DOI:**10.1038/1811199a0
29. T. Nash, *Bihem. J*. **1953**, *55*, 416–421. **DOI:**10.1042/bj0550416
30. D. J. Stueher, M. A. Marletta, *J. Immunol*. **1987**, *139*, 518–525.
31. T. Bhuyan, M. Khanuja, R. Sharma, S. Patel, M. R. Reddy, S. Anand, A. Varma, *J. Nanopart Res*. **2015**, *17*, 1–11. **DOI:**10.1007/s11051-015-3093-3
32. K. S. Ahn, T. Deutsch, Y. Yan, C. S. Jiang, C. L. Perkins, J. Turner, M. A. I. Jassim, *J Appl Phys.* **2007**, *102*, 23517–23522.
33. S. Maensiri, P. Laokul, V. Promarak, *J. Cryst. Growth*. **2006**, *289*, 102–106. **DOI:**10.1016/j.jcrysgro.2005.10.145
34. S. Suwanboon, *Sci. Asia*, **2008**, *34*, 31–34. **DOI:**10.2306/scienceasia1513-1874.2008.34.031
35. Y. C. Zhang, J. Y Jang, G. L. Wang, M. Zhang, X. Y. Hu, *J. Cryst. Growth*. **2006,** *294*, 278–282. **DOI:**10.1016/j.jcrysgro.2006.06.038
36. C. L. Xua, D. H. Qina, H. Li, Y. Guo, T. Xu, H. L. Li, *Mater. Lett.* **2004**, *58*, 3976–3979. **DOI:**10.1016/j.matlet.2004.08.026
37. M. Fua, Y. Li, S. Wu, P. Lu, J. Liu, F. Donga, *Appl Surf Sci*. **2011,** *258*, 1587–1598. **DOI:**10.1016/j.apsusc.2011.10.003
38. A. Samavati, A. F. Ismail, H. Nur, Z. Othaman, M. K. Mustafa, *Chin. Phys. B*. **2016**, *25*, 077803–077809. **DOI:**10.1088/1674-1056/25/7/077803
39. S. A. Khan, F. Noreen, S. Kanwal, A. Iqbal, G. Hussain, *Mater. Sci. Eng. C*. **2017**, *82*, 46–59. **DOI:**10.1016/j.msec.2017.08.071
40. S. Y. Pung, C. S. Ong, K. M. Isha, M. H. Othman, *Sains Malays*. **2014,** *43*, 273–281.
41. H. R. Ghaffarian, M. Saiedi, M. A. Sayyadnejad, A. M. Rashidi, *Iran. J. Chem. Chem. Eng.* **2011,** *30*, 1–6.
42. M. Premanathan, K. Karthikeyan, K. Jeyasubramanian, G. Manivannan, *Nanomedicine*. **2011**, *7*, 184–192. **DOI:**10.1016/j.nano.2010.10.001
43. K. R. Raghupathi, R. T. Koodali, A. C. Manna, *Langmuir*. **2011**, *27*, 4020–4028. **DOI:**10.1021/la104825u
44. T. Bhuyan, K. Mishra, M. Khanuja, R. Prasad, A.Varma, *Mater Sci Semicond Process*. **2015**, *32*, 55–61. **DOI:**10.1016/j.mssp.2014.12.053
45. W. K. Jung, H. C. Koo, K. W. Kim, S. Shin, S. H. Kim, Y. H. Park, *Appl Environ Microbiol*. **2008,** *74,* 2171–2178. **DOI:**10.1128/AEM.02001-07
46. M. Li, S. Pokhrel, X. Jin, L. Madler, R. Damoiseaux, E. M. V. Hoek, *Environ Sci Technol*. **2011**, *45*, 755–761. **DOI:**10.1021/es102266g

Povzetek

V prispevku preučujemo, kako dopiran baker (Cu) v nanodelcih cinkovega oksida (ZnO) vpliva na energijsko vrzel ("band gap") in na selektivno citotoksičnost napram celicam raka dojke (MCF7), celicam raka materničnega vratu (HeLa) in napram normalnim celicam (Vero). Nanodelce ZnO dopirane z Cu (Cu – ZnO NPs) smo sintetizirali in karakterizirali z UV-Vis spektroskopijo, infrardečo spektroskopijo (FT-IR), rentgensko praškovno difrakcijo (XRD), vrstično elektronsko mikroskopijo (SEM) in energijsko disperzijsko spektroskopijo rentgenskih žarkov (EDX). Energijska vrzel dopiranih nanodelcev ZnO se je zmanjšala iz 3,54 eV na 3,29 eV. Antimikrobno aktivnost smo ovrednotili napram trem bakterijskim in glivičnim sevom. Antioksidativno delovanje smo preučili z uporabo prostega radikala DPPH, radikalov $ABTS^{+}$, hidroksilnih radikalov in radikalov dušikovega oksida. Rakave celice smo izpostavili nanodelcem in izmerili vrednosti IC_{50}: 219,56 μg/ml (MCF7) in 137,27 μg/ml (HeLa). Dopirani nanodelci ZnO (Cu–ZnO NPs) imajo izboljšano selektivno citotoksičnost napram celicam MCF7 in HeLa, dopiranje pa ne vpliva na normalne celice.